Supporting Information

One-Nanometer-Thick Interfaces of Titania Nanosheets for Reversible Zn-Metal Electrodes

Chenhui Wang, Nobuyuki Sakai, Yasuo Ebina, Daiming Tang, Renzhi Ma, Takayoshi Sasaki**

Experiments

Materials: Potassium carbonate (K_2CO_3, 99.9%, Rare Metallic), titanium dioxide (TiO_2, 99.99%, Rare Metallic), lithium carbonate (Li_2CO_3, 99.99%, Rare Metallic), hydrochloric acid (HCl, 35 wt%, Kishida Chemical), tetrabutylammonium hydroxide solution (TBAOH, 10 wt%, Wako special grade, FUJIFILM Wako Pure Chemical), dimethyl sulfoxide (DMSO, Guaranteed reagent, FUJIFILM Wako Pure Chemical), zinc sulfate ($ZnSO_4$, Wako 1st grade, FUJIFILM Wako Pure Chemical), and zinc sheet (Zn, 99.98%, Alfa Aesar) were used as purchased, except for the zinc sheets that were used after polishing.

Preparation of unilamellar $Ti_{0.87}O_2$ nanosheets: The $Ti_{0.87}O_2$ nanosheets were prepared according to the procedure described in our previous reports.[1-6] Briefly, a mixture of K_2CO_3, TiO_2, and Li_2CO_3 (0.42:1.73:0.135 in molar ratio) was calcined at 1000 °C for 20 h to synthesize the layered titanate $K_{0.8}Ti_{1.73}Li_{0.27}O_4$. The obtained $K_{0.8}Ti_{1.73}Li_{0.27}O_4$ (15 g) was treated with HCl (1 mol L^{-1}, 1 L) for 3 days to obtain $H_{1.07}Ti_{1.73}O_4 \cdot H_2O$. In this process, Li ions in the host layer are extracted, leaving octahedral vacancies.[4,5] $H_{1.07}Ti_{1.73}O_4 \cdot H_2O$ (4 g) was delaminated into colloidal single layers of $Ti_{0.87}O_2^{0.52-}$ by immersion in an aqueous solution of TBAOH (1 L) with a molar ratio of $TBA^+/H^+ = 1$. After 30 days of intermittent shaking, a suspension with a milky appearance was produced. The suspension was subjected to centrifugation at 10,000 rpm for 30 min to sediment all of the nanosheets, which were redispersed in DMSO.

Flocculation of $Ti_{0.87}O_2$ nanosheets: An aqueous suspension of $Ti_{0.87}O_2$ nanosheets (2.82 g/L, 20 mL) was added into a $ZnSO_4$ solution (1 M, 20 mL). The flocculated product was washed with pure water and recovered by centrifuging at 10000 rpm followed by drying at 100 °C overnight.

Materials characterization: XRD patterns were recorded with a powder X-ray diffractometer (Rigaku, Rint-2200) using Cu Kα radiation (λ = 1.5405 Å). A zeta-potential and particle size

analyzer (Otsuka Electronics, ELSZ-2) was employed to measure the zeta potential of the aqueous suspension. AFM (Hitachi High-Tech Science, AFM5000II) was used to characterize the topography of the nanosheets. The morphologies of the electrodes were monitored with SEM (JEOL, JSM-6010LA), and the elemental composition was examined by an energy-dispersive X-ray spectrometer (EDS). In-plane XRD measurements were performed with synchrotron X-ray radiation (λ = 1.1991 Å) at line BL-6C of the Photon Factory, High Energy Accelerator Research Organization. The samples for the cross-sectional observations were prepared by a focused ion beam (FIB, Hitachi High-Tech Science, Xvision200DB) and then examined using TEM (JEOL, JEM-2100F) equipped with EDS. XPS (ULVAC-PHI, PHI 680) and time-of-flight SIMS (ULVAC-PHI, Quantera SXM) were used to identify the surface states of the samples. A contact angle meter (Kyowa Interface Science, CA-XP) was employed to assess the hydrophilicities of the materials. An optical microscope (Olympus, BX51) was used to monitor Zn deposition in real time. The resistivity of the electrodes was measured by a four-point probe resistivity meter (Mitsubishi Chemical Analytech, Loresta-GP, MCP-T610).

Fabrication of Zn-metal electrodes coated with $Ti_{0.87}O_2$ nanosheets: A monolayer film of $Ti_{0.87}O_2$ nanosheets was fabricated on the Zn surface by spin coating a DMSO suspension with a spin coater (MIKASA, MS-B100). A 2 × 2 cm^2 zinc sheet was pretreated with O_2 plasma (Vacuum Device, PIB-20) for 2 min to clean the surface before spin coating. The $Ti_{0.87}O_2$ suspension (0.1 wt%, 120 μL) was placed on the zinc substrate and then allowed to spread for 30 s. Following the initial rotation at 100 rpm for 5 s, higher speeds, 1200, 1400, or 2000 rpm, was applied for 300 s to deposit the film. The rotational speed of 1200 rpm was determined to be the optimum value for attaining full coverage of various substrate surfaces (Zn, Si, and SS) with monolayer films of neatly tiled $Ti_{0.87}O_2$ nanosheets.

Electrochemical measurements: The electrochemical experiments were carried out using an electrochemical station (Autolab, AUT87433). Linear sweep voltammetry (LSV) was performed using a three-electrode system with the electrolytes 1 M Na_2SO_4 or 1 M $ZnSO_4$, a working electrode of Zn or $Ti_{0.87}O_2$@Zn, an Ag/AgCl reference electrode, and a graphite foil counter electrode. The 2032-type coin cells were assembled in the ambient environment using a 1 M $ZnSO_4$ electrolyte, a Whatman glass fiber, and electrodes of Zn, $Ti_{0.87}O_2$@Zn, SS, or $Ti_{0.87}O_2$@SS. The performance in Zn plating/stripping was evaluated with a charging/discharging system (Hokuto, HJ1001SD8) with a Zn/Zn-based battery. The overpotential for Zn nucleation was estimated with a Zn/SS-based battery due to its high anticorrosion properties.

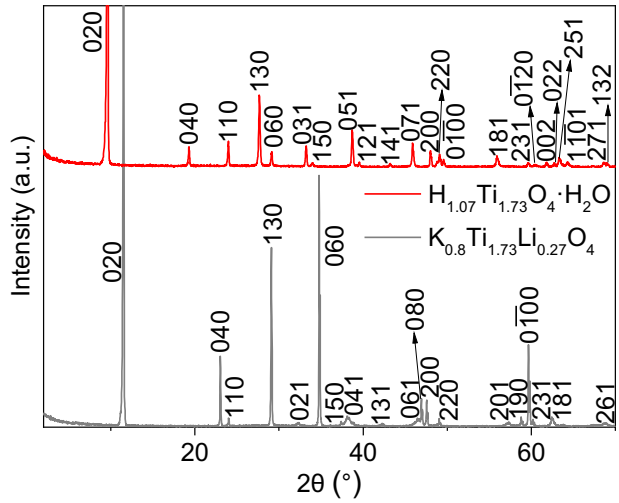

Figure S1. XRD patterns of $K_{0.8}Ti_{1.73}Li_{0.27}O_4$ and $H_{1.07}Ti_{1.73}O_4 \cdot H_2O$. The data can be indexed to orthorhombic structure with unit cell parameters of a = 0.3818(1) nm, b = 1.5471(6) nm, and c = 0.2966(2) nm for the former phase and a = 0.37839(9) nm, b = 1.8363(4) nm, and c = 0.29972(6) nm for the latter.

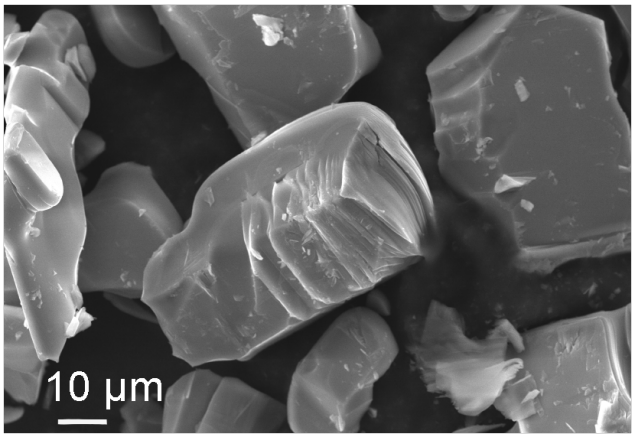

Figure S2. SEM image of $K_{0.8}Ti_{1.73}Li_{0.27}O_4$.

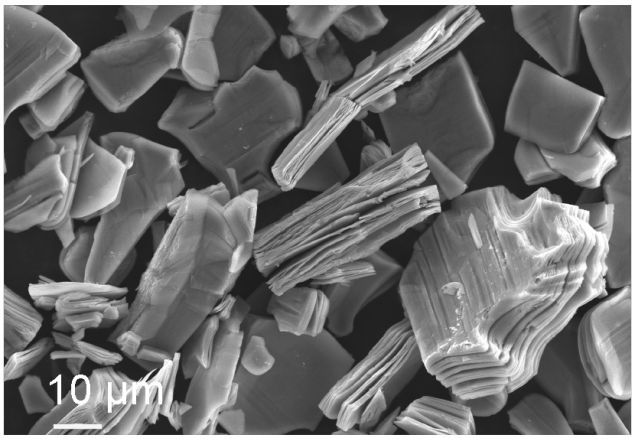

Figure S3. SEM image of $H_{1.07}Ti_{1.73}O_4 \cdot H_2O$.

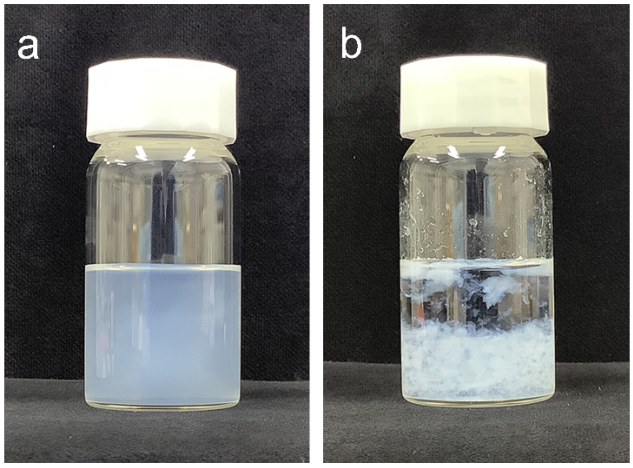

Figure S4. Pictures of (a) an aqueous suspension of $Ti_{0.87}O_2$ nanosheets and (b) that after mixing with 1 M $ZnSO_4$ solution. White flocculates are seen in (b). Elemental analysis of the flocculated product by SEM/EDS yielded the Zn/Ti ratio of 0.426 ± 0.022, which corresponds to ~0.49 Zn^{2+} per formula weight of $Ti_{0.87}O_2$ nanosheets.

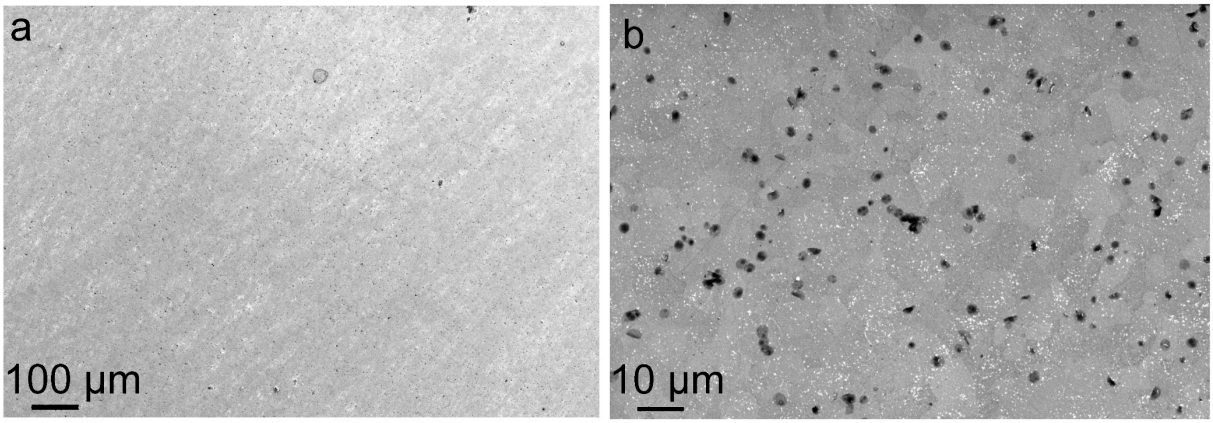

Figure S5. SEM images of (a) polished bare Zn surface and (b) its enlargement. The dark spots are the pits on Zn surface.

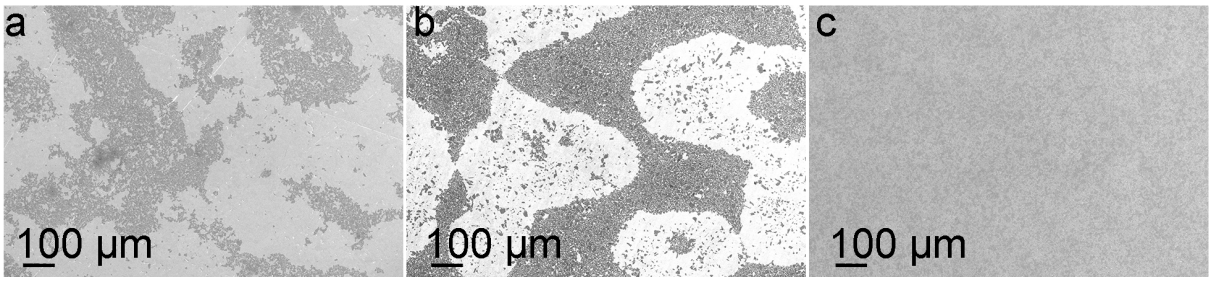

Figure S6. SEM images of $Ti_{0.87}O_2$@Zn prepared by spin coating at (a) 2000 rpm, (b) 1400 rpm, and (c) 1200 rpm with the $Ti_{0.87}O_2$ nanosheets (0.1 wt%) dispersed in DMSO. Dark zone corresponds to the area where the nanosheets are deposited in a neatly tiled monolayer, while

brighter region corresponds to the area without nanosheets.

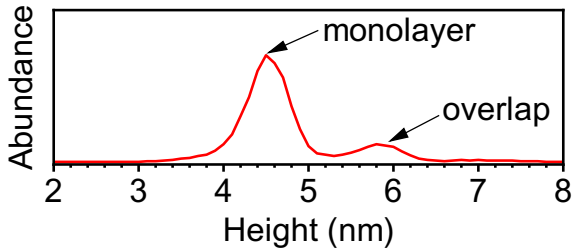

Figure S7. Height histogram of the AFM image shown in Figure 1b.

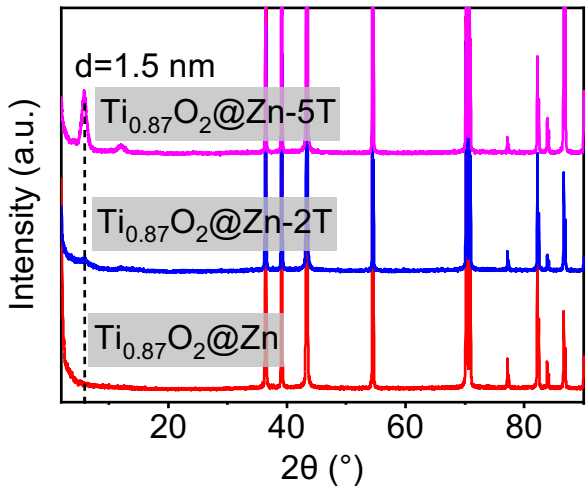

Figure S8. XRD data of $Ti_{0.87}O_2$@Zn with different times of spin coating (1 time: $Ti_{0.87}O_2$@Zn; 2 times: $Ti_{0.87}O_2$@Zn-2T; and 5 times: $Ti_{0.87}O_2$@Zn-5T).

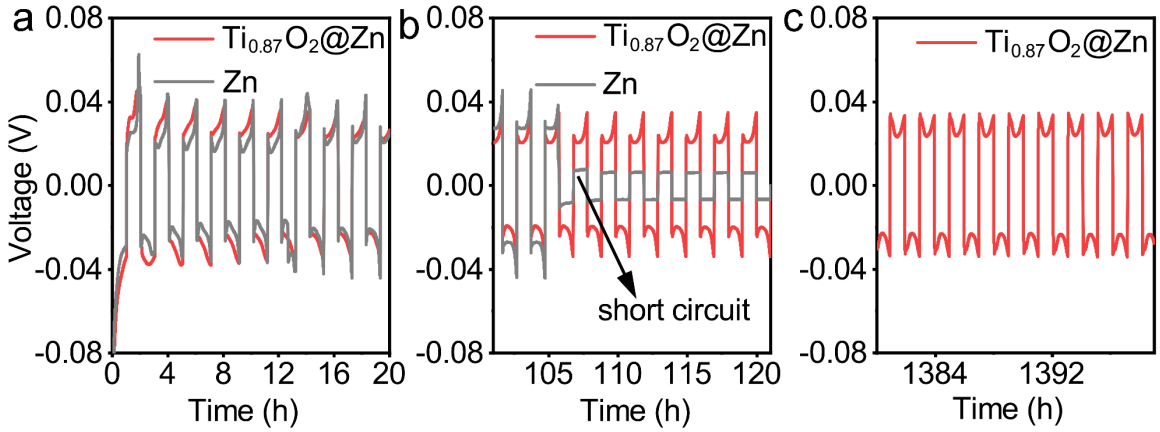

Figure S9. Galvanostatic charge/discharge curves of Zn/Zn and $Ti_{0.87}O_2$@Zn/$Ti_{0.87}O_2$@Zn symmetric batteries at a current density of 1 mA cm^{-2} and capacity of 1 mAh cm^{-2} in different periods: (a) 0–20 h; (b) 100–120 h; and (c)1380–1400 h.

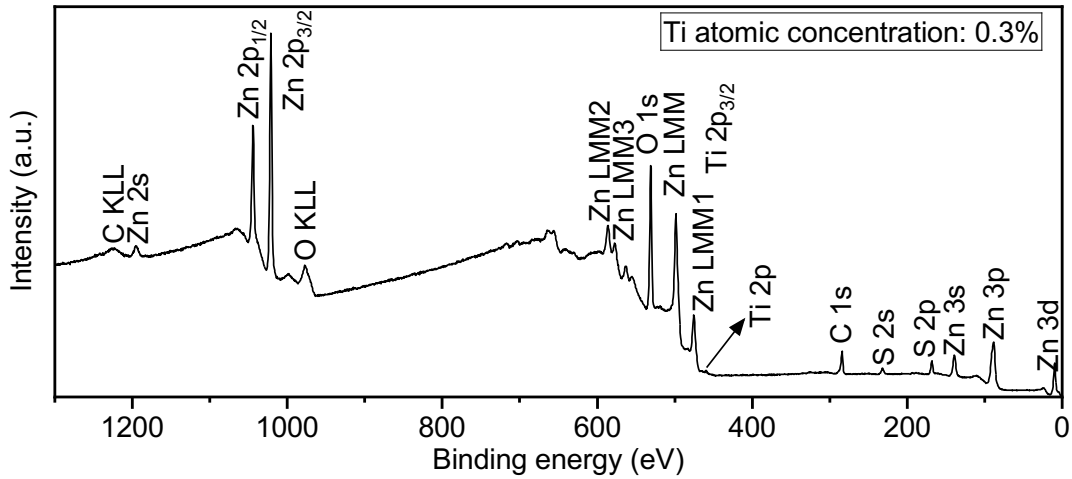

Figure S10. XPS survey spectra of the $Ti_{0.87}O_2$@Zn after Zn deposition.

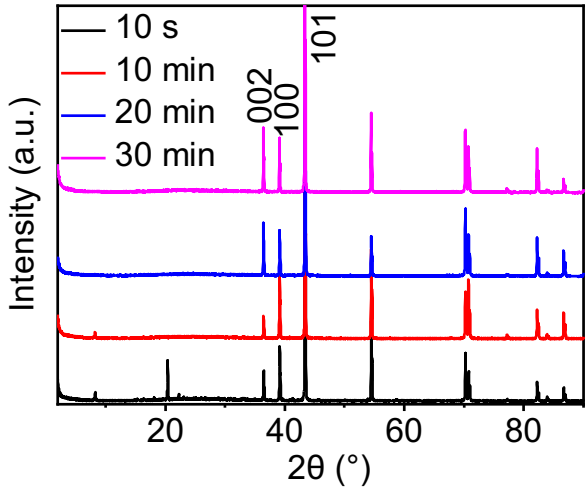

Figure S11. XRD patterns of the $Ti_{0.87}O_2$@Zn after Zn deposition for the indicated periods. The intensity of the 002 peak became highly while that of others remained substantially unchanged.

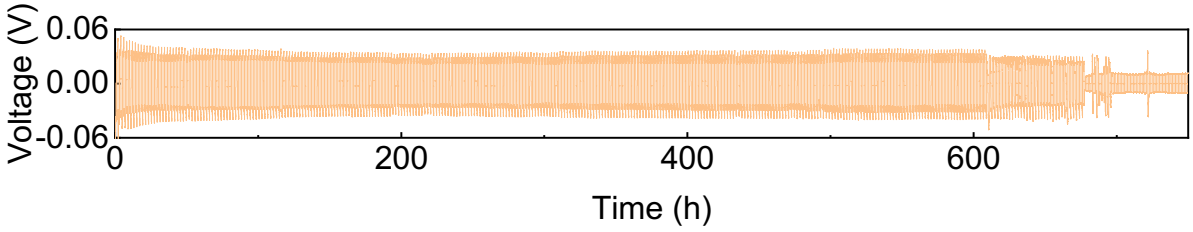

Figure S12. Galvanostatic charge/discharge curves of $Ti_{0.87}O_2$@Zn-2T/$Ti_{0.87}O_2$@Zn-2T symmetric batteries at a current density of 1 mA cm^{-2} and capacity of 1 mAh cm^{-2}.

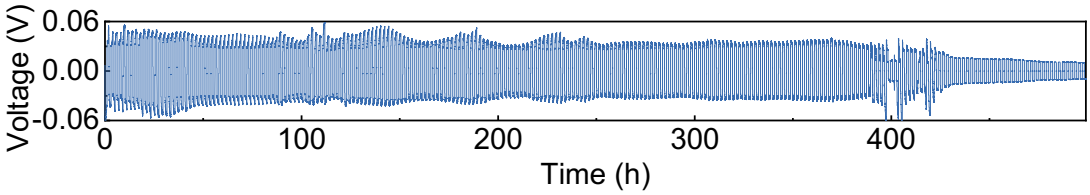

Figure S13. Galvanostatic charge/discharge curves of $Ti_{0.87}O_2$@Zn-5T/$Ti_{0.87}O_2$@Zn-5T symmetric batteries at a current density of 1 mA cm^{-2} and capacity of 1 mAh cm^{-2}.

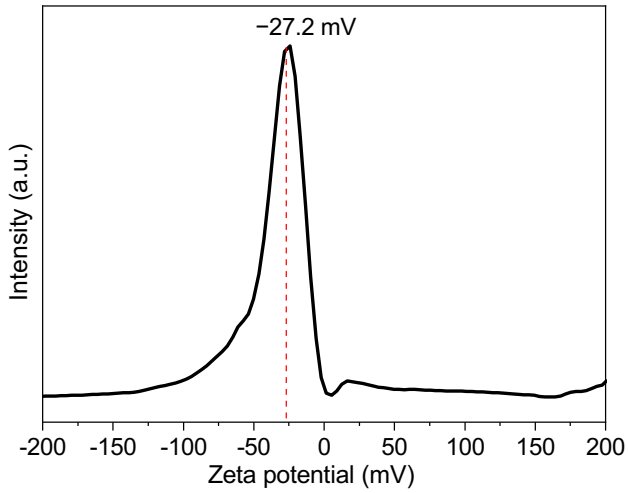

Figure S14. Zeta potential of the aqueous suspension of $Ti_{0.87}O_2$ nanosheets.

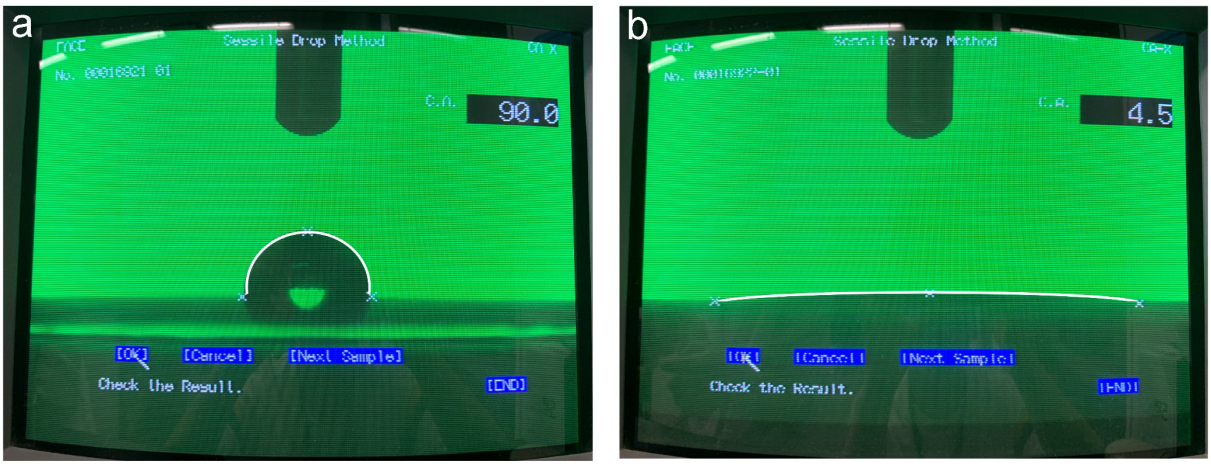

Figure S15. Photographs of a water droplet on the surface of (a) Zn and (b) $Ti_{0.87}O_2$@Zn. While a water droplet on the Zn surface showed a hemispherical shape with a contact angle of 90°, a water droplet spread out on the $Ti_{0.87}O_2$@Zn surface with a contact angle of 4.5°.

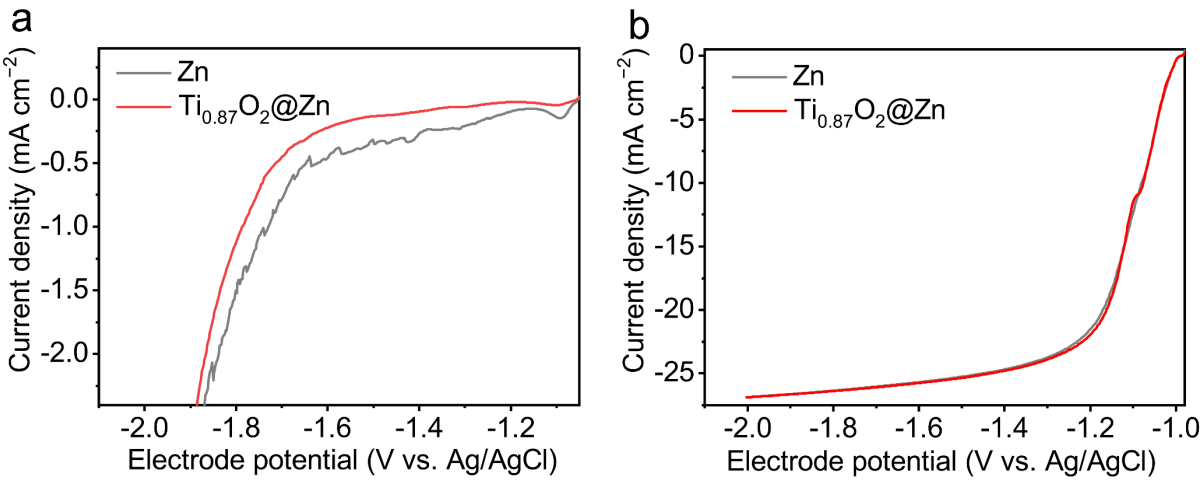

Figure S16. LSV curves of Zn and $Ti_{0.87}O_2$@Zn electrodes in the electrolyte solution of (a) 1 M Na_2SO_4 and (b) 1 M $ZnSO_4$ at the sweep rate of 1 mV s^{-1}.

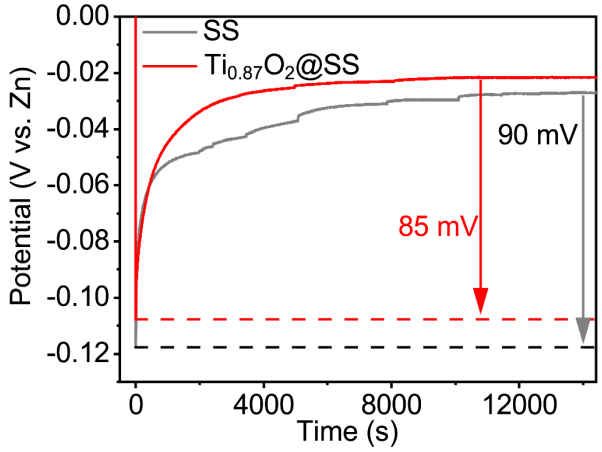

Figure S17. Potential changes during Zn plating on SS electrode in the Zn/SS battery and $Ti_{0.87}O_2$@SS electrode in the Zn/$Ti_{0.87}O_2$@SS battery at 1 mA cm^{-2}.

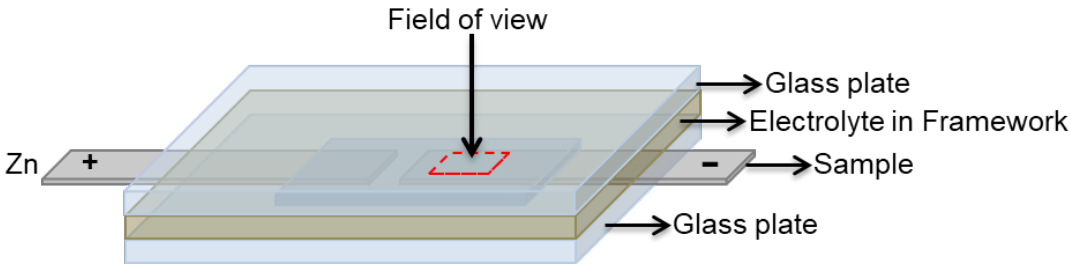

Figure S18. Schematic diagram of a homemade setup for in situ microscope observation.

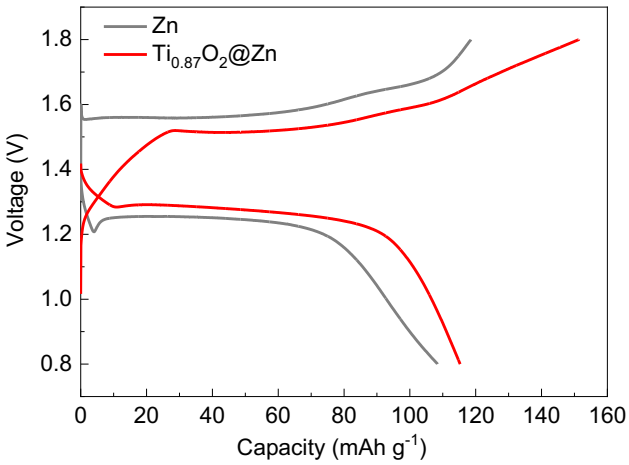

Figure S19. Galvanostatic charge/discharge curves of Zn-MnO_2 full cell with the bare Zn anode or the $Ti_{0.87}O_2$@Zn anode at 0.05 A g^{-1}. Electrolyte: 1 M $ZnSO_4$.

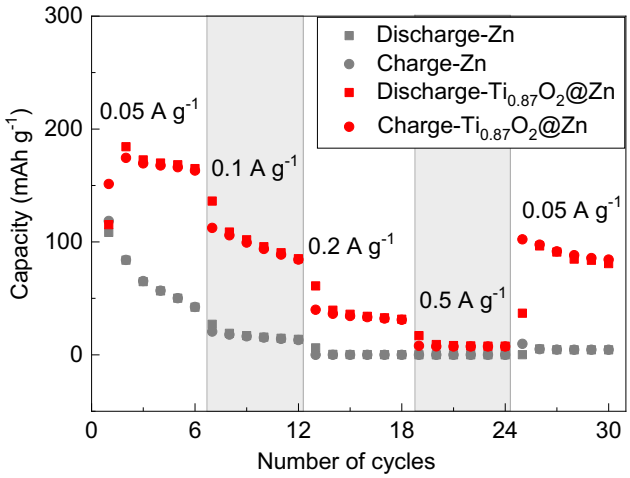

Figure S20. Rate performance of Zn-MnO_2 full cell with the bare Zn anode or the $Ti_{0.87}O_2$@Zn anode. Electrolyte: 1 M $ZnSO_4$.

Captions for Movies:

Movie S1. In situ microscope observation of the deposition process of Zn on a Zn electrode surface in 1 M $ZnSO_4$ at −10 mA cm^{-2}. The area where Zn is deposited became dark upon applying the current and a number of small particles appeared, while some regions remained bright, indicating that the Zn deposition rate was locally dependent.

Movie S2. In situ microscope observation of the deposition process of Zn on a $Ti_{0.87}O_2$@Zn electrode surface in 1 M $ZnSO_4$ at −10 mA cm^{-2}. All area became dark upon applying the current and a number of small particles appeared, showing a uniform distribution of the Zn deposition rate.

Table S1. Comparison of the interfaces for Zn electrodes.

Interface material	Thickness	Cycle life (h)	Current density (mA cm^{-2})	Areal capacity (mAh cm^{-2})	Binder	Ref.
Hydrogen-substituted graphdiyne	500 nm	2400	2	0.1	None	[7]
Nano-$CaCO_3$	5 μm	400	0.25	0.05	Polyvinylidene difluoride	[8]
Imidazolate framework-8	1 μm	1200	2	1	None	[9]
Zn-based montmorillonite	1.5-5 μm	1000	1	0.25	Polyvinylidene difluoride	[10]
Kaolin $Al_2Si_2O_5(OH)_4$	20 μm	800	4.4	1.1	Polyvinylidene difluoride	[11]
Poly(vinyl butyral)	4 μm	2200	0.5	0.5	None	[12]
ZrO_2	μm-scale	3600	0.25	0.125	Polyvinylidene difluoride	[13]
$NaTi_2(PO_4)_3$	20-25 μm	250	1	1	Polyvinylidene difluoride	[14]
Alucone	12 nm	780	3	1	None	[15]
$Ti_3C_2T_x$	100-200 nm	820	0.2	0.2	None	[16]
TiO_2	8 nm	140	1	1	None	[17]
$Ti_{0.87}O_2$	1 nm	1400	1	1	None	This work

Table S2. Resistivity of bare Zn electrodes and those coated with $Ti_{0.87}O_2$ nanosheets.

Electrode	Zn	$Ti_{0.87}O_2$@Zn	$Ti_{0.87}O_2$@Zn-2L	$Ti_{0.87}O_2$@Zn-5L
Resistivity (10^{-8} Ω m)	9.5	14	14	15

References

(1) Sasaki, T.; Watanabe, M.; Michiue, Y.; Komatsu, Y.; Izumi, F.; Takenouchi, S. Preparation and Acid-Base Properties of a Protonated Titanate with the Lepidocrocite-like Layer Structure. *Chem. Mater.* **1995**, *7*, 1001-1007.

(2) Sasaki, T.; Komatsu, Y.; Fujiki, Y. A new layered hydrous titanium dioxide $H_xTi_{2-x/4}O_4 \cdot H_2O$. *J. Chem. Soc., Chem. Commun.* **1991**, 817-818.

(3) Sasaki, T.; Watanabe, M.; Hashizume, H.; Yamada, H.; Nakazawa, H. Macromolecule-like Aspects for a Colloidal Suspension of an Exfoliated Titanate. Pairwise Association of Nanosheets and Dynamic Reassembling Process Initiated from It. *J. Am. Chem. Soc.* **1996**, *118*, 8329-8335.

(4) Sasaki, T.; Watanabe, M. Osmotic Swelling to Exfoliation. Exceptionally High Degrees of Hydration of a Layered Titanate. *J. Am. Chem. Soc.* **1998**, *120*, 4682-4689.

(5) Sasaki, T.; Kooli, F.; Iida, M.; Michiue, Y.; Takenouchi, S.; Yajima, Y.; Izumi, F.; Chakoumakos, B. C.; Watanabe, M. A Mixed Alkali Metal Titanate with the Lepidocrocite-like Layered Structure. Preparation, Crystal Structure, Protonic Form, and Acid−Base Intercalation Properties. *Chem. Mater.* **1998**, *10*, 4123-4128.

(6) Maluangnont, T.; Matsuba, K.; Geng, F.; Ma, R.; Yamauchi, Y.; Sasaki, T. Osmotic Swelling of Layered Compounds as a Route to Producing High-Quality Two-Dimensional Materials. A Comparative Study of Tetramethylammonium versus Tetrabutylammonium Cation in a Lepidocrocite-type Titanate. *Chem. Mater.* **2013**, *25*, 3137-3146.

(7) Yang, Q.; Guo, Y.; Yan, B.; Wang, C.; Liu, Z.; Huang, Z.; Wang, Y.; Li, Y.; Li, H.; Song, L.; Fan, J.; Zhi, C. Hydrogen-Substituted Graphdiyne Ion Tunnels Directing Concentration Redistribution for Commercial-Grade Dendrite-Free Zinc Anodes. *Adv. Mater.* **2020**, *32*, 2001755.

(8) Kang, L.; Cui, M.; Jiang, F.; Gao, Y.; Luo, H.; Liu, J.; Liang, W.; Zhi, C. Nanoporous $CaCO_3$ Coatings Enabled Uniform Zn Stripping/Plating for Long-Life Zinc Rechargeable Aqueous Batteries. *Adv. Energy Mater.* **2018**, *8*, 1801090.

(9) Liu, X.; Yang, F.; Xu, W.; Zeng, Y.; He, J.; Lu, X. Zeolitic Imidazolate Frameworks as Zn^{2+} Modulation Layers to Enable Dendrite-Free Zn Anodes. *Adv. Sci.* **2020**, *7*, 2002173.

(10) Yan, H.; Li, S.; Nan, Y.; Yang, S.; Li, B. Ultrafast Zinc-Ion-Conductor Interface toward High-Rate and Stable Zinc Metal Batteries. *Adv. Energy Mater.* **2021**, *11*, 2100186.

(11) Deng, C.; Xie, X.; Han, J.; Tang, Y.; Gao, J.; Liu, C.; Shi, X.; Zhou, J.; Liang, S. A Sieve-Functional and Uniform-Porous Kaolin Layer toward Stable Zinc Metal Anode. *Adv. Funct. Mater.* **2020**, *30*, 2000599.

(12) Hao, J.; Li, X.; Zhang, S.; Yang, F.; Zeng, X.; Zhang, S.; Bo, G.; Wang, C.; Guo, Z. Designing Dendrite-Free Zinc Anodes for Advanced Aqueous Zinc Batteries. *Adv. Funct. Mater.* **2020**, *30*, 2001263.

(13) Liang, P.; Yi, J.; Liu, X.; Wu, K.; Wang, Z.; Cui, J.; Liu, Y.; Wang, Y.; Xia, Y.; Zhang, J. Highly Reversible Zn Anode Enabled by Controllable Formation of Nucleation Sites for Zn-Based Batteries. *Adv. Funct. Mater.* **2020**, *30*, 1908528.

(14) Liu, M.; Cai, J.; Ao, H.; Hou, Z.; Zhu, Y.; Qian, Y. $NaTi_2(PO_4)_3$ Solid-State Electrolyte Protection Layer on Zn Metal Anode for Superior Long-Life Aqueous Zinc-Ion Batteries. *Adv. Funct. Mater.* **2020**, *30*, 2004885.

(15) He, H.; Liu, J. Suppressing Zn dendrite growth by molecular layer deposition to enable long-life and deeply rechargeable aqueous Zn anodes. *J. Mater. Chem. A* **2020**, *8*, 22100-22110.

(16) Zhang, N.; Huang, S.; Yuan, Z.; Zhu, J.; Zhao, Z.; Niu, Z. Direct Self-Assembly of MXene on Zn Anodes for Dendrite-Free Aqueous Zinc-Ion Batteries. *Angew. Chem. Int. Ed.* **2020**, *60*, 2861-2865.

(17) Zhao, K.; Wang, C.; Yu, Y.; Yan, M.; Wei, Q.; He, P.; Dong, Y.; Zhang, Z.; Wang, X.; Mai, L. Ultrathin Surface Coating Enables Stabilized Zinc Metal Anode. *Adv. Mater. Interfaces* **2018**, *5*, 1800848.